RSC Advances

ROYAL SOCIETY OF CHEMISTRY

www.rsc.org/advances

Cite this: DOI: 10.1039/c0xx00000x

www.rsc.org/xxxxxx

PAPER

Development of Biocompatible Nanocubes as a T_1-Contrast Enhancer for MR Imaging of Primary and Metastatic Liver Cancer

Xiao-xia Song,[a] Xian-zhu Xu,[b] Hong-ping Wan,[a] and Qun Tang*[a]

Received (in XXX, XXX) Xth XXXXXXXXX 20XX, Accepted Xth XXXXXXXXX 20XX

DOI: 10.1039/b000000x

In this paper T_1 contrast agent-enhanced Magnetic Resonance Imaging of hepatic lesions in vivo was systematically investigated using dextran-coated $KMnF_3$ nanocubes, a new type of contrast enhancer that we have developed recently. The water-soluble nanocubes were simply synthesized via solution method. They showed good crystallinity and high r_1 relaxivities (12 $mM^{-1}\cdot s^{-1}$). Cellular nanotoxicity issues including cell proliferation, oxidative stress and cell membrane integrality were evaluated, and all the results confirmed the dextran-coated $KMnF_3$ nanocubes are highly biocompatible within the test concentrations. In vivo organ distribution showed it was predominantly taken up by liver and spleen, and excluded out of the main organs within appropriate residual time. Histopathology of the six main organs harvested within three days postinjection yielded no significant signs of tissue damage. Hematology and blood chemistry analysis further proved its high hemo-compatibility and in vivo biocompatibility. In vivo nanocube-enhanced hepatic MRI was applied for primary liver and metastatic liver cancer of mouse model, clear tumor contrast was achieved for both types of liver cancer, enabling the lesions as small as 0.4 mm to be detected. The liver cancer was confirmed by pathological section.

Introduction

Liver cancer includes primary liver cancer, also known as hepatocellular carcinoma (HCC) and metastatic liver cancer from other organs (e.g. colorectal cancer (CRC) liver metastasis). Early diagnosis of small liver lesions is correlating with clinically improved survival rates regardless of primary or metastatic cancer. Liver is known for its enrichment with mononuclear-phagocytic cells. Therefore, in the past years continuous efforts aiming to enhance visibility of liver lesions have been particularly focusing on the development of mononuclear-phagocytic-system (MPS)-entrapped agents.[1] Excitable nanoparticles (NPs) with appropriate sizea have been the dominant candidate for in vivo liver imaging during decades and it is still expanding nowadays. [2]

Two nanostructural features as MPS-targeted MRI contrast enhancer are well developed: superparamagnetic iron oxide nanoparticle (SPIO) and paramagnetic liposome.[3] As the T_2 agents SPIOs are considered to be taken up by the MPS after intravenous injection, primarily via phagocytosis by Kupffer cells, the resident liver macrophages, in the liver sinusoid, whereas there lacks of Kupffer cells in all types of cancer tissues. Dextran-coated SPIO (ferumoxides) has been applied as the first nanoparticle-based imaging agent for the detection of liver lesions.[4] However, the fate of iron oxide as hepatic contrast agents remains unclear as some of the SPIO products have recently been withdrawn in USA and Europe.[5] Moreover, metastatic liver cancer presents diagnostic challenge due to their smaller size, higher dispersion to organs, and lower vascularization than primary tumors, which make them less accessible to nanoparticle agents,[6] exceptionally, some groups reported target-imaging or therapy of metastasis via SPIO-enhanced MRI.[7] Additionally, passive target to liver by the well-known MPS effect is still the most promising way, as active target to the cancer via bio-recognition, sometimes, lost its target function during its circulation in vivo.[8] Moreover, the dark signal in T_2-weighted MRI can mislead the clinical diagnosis. Therefore, biocompatible paramagnetic nanoparticles with high relaxivity and predominant uptake by liver MPS system have possibility to be efficient T_1 hepatic contrast agent.

Recently, some paramagnetic nanomaterials (e.g. MnO, Gd_2O_3) are newly developed as T_1 contrast agent.[9] However, some critical issues such as unknown toxicity, in vivo relaxivity, and pharmacokinetics) need to be fully addressed before its application for cancer diagnosis. Until now few specific T_1 hepatic nanoparticular contrast agent was reported. We have recently introduced anti-ferromagnetic $KMnF_3$ nanocube (NC) as a new type of T_1 contrast agent with ultra-high relaxivity, proper plasma retention time and enhanced MR imaging of subcutaneous tumor.[10] In this paper, we systematically study dextran-coated $KMnF_3$ NC as a hepatic contrast enhancer. In vitro cellular toxicity and in vivo distribution were evaluated carefully after chemical synthesis and analysis. Two typical liver cancer models named as chemical-induced HCC and CRC liver metastases were established. The NCs remarkably enhanced MRI contrast of both types of liver cancer. Commercial liver diagnostic T_1 agent, Mangafodipir trisodium (MnDPDP), was tested for comparison.

Experimental procedures

1 Dextran-coated $KMnF_3$ Nanocube: Preparation and Characterizations

Oleylamine-passivated monodisperse $KMnF_3$ nanocubes with the uniformly width of 15-20 nm were prepared using a previously reported method. [10c] For the ligand exchange, 1 mL of oleylamine -coated monodisperse $KMnF_3$ nanocubes in chloroform (10 mg/mL) was mixed with 1 mL of dextran in DMSO (20 mg/mL). The mixture was shaken overnight. After centrifugation, the precipitate was rinsed with ethanol three times and dispersed in 1 mL of deionized water. TEM images were obtained using a JEOL 2000EX transmission electron microscope. Hydrodynamic size was tested using a Malvern (Worcestershire, UK) Zetasizer ZS90 from three measurements of z-average diameters of the NCs. In vitro MR relaxivity was measured with 3 T Siemens MR Scanner at room temperature.

2 MTT assay and Trypan staining

In vitro cytotoxicity of the dextran-coated nanocube was assessed by the 3-(4,5-dimethylthiazol-2-yl)-2,5-iphenyltetrazolium bromide (MTT) assay. Kidney and liver cell were extracted from newborn mouse and plated in 96-well flat-bottom microplates at 10000 cells in 100 μL DMEM mediumper well. After 24 h incubation at 37 °C, the medium was replaced with 100μL serum-free DMEM medium containing NCs. Three tested groups were subject to different concentrations of Mn (the final equivalent Mn concentrations were 10, 1, and 0.1mM Mn/L). For the control group, the same volume of culture medium without NCs was used. After 24 h incubation at 37 °C, the NC suspension was removed and the cells were washed twice with PBS, and then 10 μL MTT solution was added to each well. The cells were incubated for another 4 h, and then, the supernatant was removed and 150 μL DMSO was added to each well to dissolve the formazan crystals. Finally, a microplate reader was used to measure the absorbance of all the samples. Cell viabilities were determined by comparing the absorbance of the cells incubated with/without the NCs. Trypan blue staining procedure was performed following the standard protocol. In breif, kidney and liver cells (10^5/ml) in serum-free DMEM medium were incubated with the NCs for 24 h at 37 °C, and the final added Mn ion concentration is 1mM. The cells were incubated with trypan blue dye for 1 – 2 minutes at room temperature. The cell viability was evaluated by couting the blue stained nonviable cells.

3 Oxidative stress

The formation of intracellular ROS was measured via monitoring the increasing fluorescence of 2′,7′-dichlorofluorescein (DCF). The cell-permeant H_2DCFDA, enters the cell where intracellular esterase cleave off the diacetate group. The resulting H_2DCF is retained in the cytoplasm and oxidized to DCF by ROS. 1×10^4 liver cells or 1×10^4 kidney cells were seeded into each well of a 96-well plate (100 μL) in DMEM containing 10% fetal bovine serum for 24 h. Subsequently, the cells were washed once with PBS and treated with nanocubes at a final Mn concentration of 1 mM in serum-free DMEM medium. After the incubation for 24 h, the cells were washed with PBS and incubated with 50μmol/L H_2DCFDA for 40 min. The cells were then washed with PBS to eliminate free H_2DCFDA. After a further incubation in HBSS for 1 h the fluorescence intensity was measured using the fluorescence reader (MWG-BiotechAG, Ebersberg, Germany) with an excitation wavelength of 488 nm and emission wavelength of 530 nm peak. Positive control was carried out via oxidation of H_2DCFDA by H_2O_2 with in PBS.

4 Organ distributions and Hematological analysis

All the animal experiments were conducted in conformity with Institutional guidelines for the care and use of laboratory animals in Nanchang University, and conformed to the National Institutes of Health Guide for Care and Use of Laboratory Animals. Six-week old ICR mice were purchased with the weight from 20 to 22 grams. The mice were randomly grouped (n=6) and were injected with dextran-coated nanocubes through a tail vein at dose of 5 mmol Mn/kg or saline as the control under anesthesia. At different points (0.5, 2, 12, 48 and 96 h) post-injection, the mice were sacrificed and perfused with saline, and six main organs (brain, heart, lung, spleen, liver and kidney) were collected and homogenized with nitro-hydrochloride acid. A 100 μL blood was also collected from the periorbital plexus under anesthesia through a heparinized capillary tube at each of the above time points, and resolved by nitro-hydrochloride acid. Mn ions in the organs and blood samples were analyzed using an ICP-MS or ICP-AES (Agilent 7700).

5 Whole blood assay

A subset of the mice injected with dextran-$KMnF_3$ NCs or saline at a dose of 5 mmol/kg (n = 3 per group) were used in this study. As described above, blood was collected from the periorbital plexus at defined time points after injection and transferred into EDTA containing polypropylene microtubes (Becton Dickinson). Blood samples were analyzed using a Hemavet 850FS Multi Species Hematology System (Drew Scientific) programmed with mouse hematology settings. For blood chemistries, up to around 0.8 mL of blood was quickly withdrawn by cardiac puncture under anesthesia using a 1 mL plastic syringe with a 25 gauge needle before sacrifice. After 4 hours, blood serum was separated by centrifugation at the speed of 3500 rpm for 15 min. All the blood chemical indexes were simultaneously measured in the serum by blood biochemical analyzer (TC6020).

6 Histopathology

For the histopathology studies, the standard hematoxylin-eosin (H&E) staining protocol was exploited to evaluate the possible organ toxicity caused by the injected NP. Specimens were fixed in 10% buffered formalin and embedded in paraffin. After cutting 4 μm serial sections the H&E staining was performed. Sections were evaluated for various pathologic parameters using a light microscope. Each mouse was monitored for 3 days after injection of NC nanoparticles (5 mmol Mn/kg) and compared with saline as control (n = 3 per group). The sections of all the six tissues

harvested from the mice 0.5 hour to 3days after injection were stained with and then examined by optical microscopy.

7 Primary Hepatic Cancer Model

Two-week-old mice were injected ip with a single dose of DEN (100mg/kg of body weight). After a treatment-free interval of 2 weeks mice were intragastrically administrated with 2-acetylamino- fluorene (2-AAF, dissolved in olive oil, 20 mg/kg), and repeated two weeks later. And then feed under normal condition. All the mice were kept on a 12 h dark/light cycle and had access to food and tap water ad libitum. Six months later all the mice were examined by MRI. After acquiring images the mice were sacrificed and livers were excised and immediately frozen in liquid nitrogen for pathology.

8 Colorectal Cancer Liver Metastasis Model

Colorectal cancer cell SW480 cells were maintained in RPMI-1640 medium supplemented with 10% fetal calf serum, 100 U/ml of penicillin and 100 μg/ml of streptomycin (referred to as "complete medium"). Cell cultures were kept in a humidified incubator at 37°C with 5% CO_2. Induction of colorectal liver metastases by splenic injection was preceded as follows: Under anesthesia, the abdominal cavity was opened by a 0.5 cm left sided transverse laparotomy. The spleen was identified and lifted up by a cotton wool tip. 5×10^5 SW480 cells in a total volume of 50 μl of PBS were injected subcapsularly into the spleen using a 27 gauge needle. A cotton wool tip was pressed onto the injection site for 30 seconds to prevent the leakage of cancer into the cavity. The closure of the abdominal cavity and post surgical pain relief were carried out as above. No surgery related fatalities was seen following this spleen injection procedure.

9 In vivo MRI and pathological section

MR imaging was performed using a Siemens 3.0 Tesla whole body clinical MR scanner. MR images were acquired using a spin-echo T_1-weighted MRI sequence (TR/TE = 549/16 ms, slice thickness = 0.6 mm, FOV = 24 × 49, matrix size = 192 × 384) and evaluated by considering the brightness ratio. To enhance the visibility of small lesions, slice thickness was set as the lowest limitation of 0.6 mm. The tumor-bearing mice were anesthetized and then dextran coated $KMnF_3$ NC solution was injected intravenously with Mn dosage of 5 mmol per kg. For the control group, the same dosage of MnDPDP was injected into a tail vein. After MR images were acquired, all the mice were sacrificed for pathological examination. The procedure follows standard hematoxylin-eosin staining protocol.

Results and Discussion

Size-uniformed $KMnF_3$ NCs were synthesized as reported previously.[10] Biocompatible dextran was immobilized on the surface of the NC via ligand exchange in bipolar DMSO solvent, rending the NCs water-soluble without detectable aggregation for weeks. The typical transmission electrical microscopy (TEM) images of dextran-coated $KMnF_3$ NCs are shown in Figure 1a. More than 95% of the particles of the as-obtained $KMnF_3$ were shaped with a regular cube with a mean edge length of 20-25 nm from 300 measured particles. The crystallinity of the NCs was investigated by high resolution TEM and corresponding selected area electron diffractions (SAED) on a single particle, and both indicated that each particle was a single crystal (Figure 1b). A Fourier transform infrared (FTIR) spectrum of the NCs is shown in Figure 1c. The surface coating of dextran was evidenced from the characteristic band at 1080 cm^{-1}, corresponding to the large proportion of the primary C-OH groups 'stretching vibration of the coated dextran.[11] Hydrophilic dextran-coated NC has a stable hydrodynamic diameter of around 120 nm (Figure.S1). To evaluate the T_1 enhancing capability of the dextran-coated NC, in vitro relaxivity was measured with various Mn ions concentration at room temperature under the magnetic field of 3 Tesla. T_1 relaxivity of the NC in aqueous solution is 12 $mM^{-1}\cdot s^{-1}$ by calculation the slope of the R (1/T) versus Mn concentration plots (Figure 1d). Taken together, the dextran-coated $KMnF_3$ NCs can be simply synthesized and greatly enhance signal on T_1-weighted sequences.

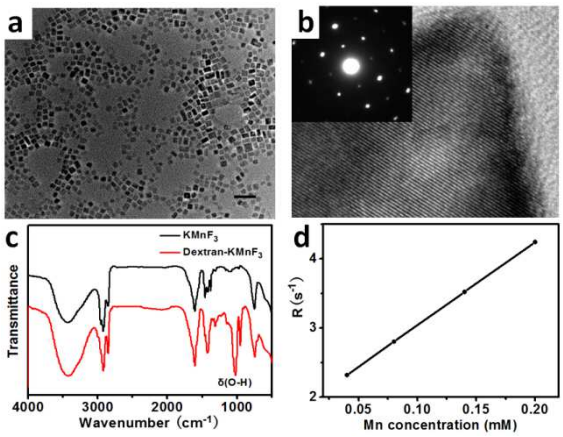

Fig. 1 (a) TEM image of the dextran-coated $KMnF_3$ NCs with well-dispersion, scale bar 50 nm. (b) HRTEM image of an individual NC with a clearly resolved lattice fringe and corresponding SAED pattern. (c) FT-IR spectra of untreated and dextran-coated $KMnF_3$ NCs. (d) Plot of the R_1 relaxation time of the dextran-coated $KMnF_3$ nanocube solutions as a function of Mn concentration obtained high r_1 value of 12 $mM^{-1}.s^{-1}$.

To evaluate the NC's cytotoxicity, liver and kidney cells extracted from newborn mouse were incubated with various concentrates of NC solution at ambient temperature. Cell viability, expressed as the percentage of viable cells compared with controls, was evaluated using the MTT (3-(4,5-dimethylthiazol-2-yl)-2,5-diphenyltetrazolium bromide) assay. The cell viability was able to maintain up to around 95% as the Mn concentration was 0.1 mM and 1 mM. With the concentration was elevated to 10 mM, the viability dropped rapidly to 50% for both type of cells, indicating its cellular toxicity only at high Mn concentration (Figure 2a). Trypan blue staining further confirmed that the cells were able to maintain the integrity of cell membrane after exposure for 12 hrs (Figure S2). Reactive oxygen species (ROS) are well-known for their roles on many critical signaling pathways in cells. ROS generation is one of the most frequently reported NP-associated toxicities. Free ferric iron degraded from SPIO was found in some cases to induce high levels of ROS,

resulting in apoptosis or inflammation.[12] 2′,7′-dichlorofluorescin diacetate (DCFDA) is one of the mostly used probes for ROS detection as it can be oxidized into luminescent 2′,7′-dichlorofluorescien (DCF) by oxidative species, which is reflected as a peak emission at 530 nm. [13] As presented in Figure 2b there is no ROS production in both cells incubated with dextran-coated NCs for 24 hours.

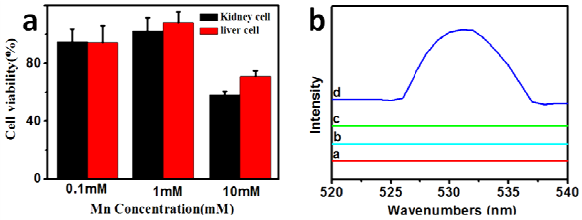

Fig. 2 (a) Liver and kidney cell viability for dextran-coated NCs at various Mn concentrations of dextran-coated NCs. (b) Luminescent spectrum of the probes with NCs as it was incubated in saline (a), kidney cell (b), liver cell (c), and H_2O_2 solution (0.1 M) as comparison (d).

We next evaluated the in vivo biodistribution and clearance of dextran-coated nanocube in mice, as shown in Figure 3a. The results indicate that most of the nanocubes were accumulated predominantly in the liver and spleen after injection, but were cleared from the organs after two days. Thirty minutes after injection, the NC' concentration in the liver and spleen was maximally 9 μg/g and 8 μg/g, respectively. Accumulation in all the major organs decreased with time, and two days later it basically returned to the pre-injected level. It was also noted that small fractions of nanocubes were distributed into the kidney, maximally at 5 μg/g, while a total of only 1-2 μg/g increments were detected in other organs (e.g. heart and brain). Moreover, there was no significant change in Mn contents observed in the lung before and after injection. Plasma retention curve showed that the circulation half-life of the NCs is approximately two hours (Figure 3b). The favorable retention time suggests the suitability of the NCs serving as an in vivo diagnostic agent.

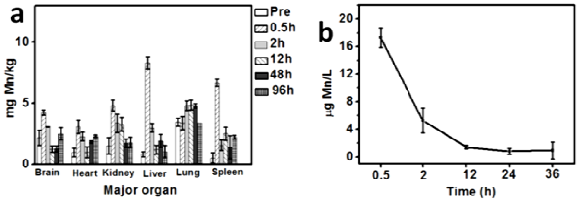

Fig. 3 (a) Biodistribution of dextran-coated $KMnF_3$ NCs, in the major organs of the ICR mouse mice including brain, heart, kidney, liver, lung, spleen. The data was recorded from whole organ taken at indicated times after injection. (b) Eliminated curve of dextran-coated $KMnF_3$ NCs in the plasma. Both tests had the same dosages as 5mmol/kg.

All six organs of those mice were simultaneously excised and their pathological sections were analyzed to evaluate the possible toxicity of the NC. Hematoxylin and Eosin (H&E) staining was performed on all sections. As shown in Figure 4, the surrounding alveolar walls, blood vessel of heart, kidney, spleen and liver are occasionally dilated, and rarely hydroncus was detected in the brain, lung. No inflammatory response was defined in all the organs within three days after injection. NPs have been reported to detect and alleviate allergy symptoms, such as inflammation, and also act as inducers of the immune response, sometimes. Their immunocompatibility depends on the materials, size, surface chemistry, as well as the cell type.[14] Undetectable pathology were found on the six main organs, which indicates that in vivo toxicity might be minimal which is possibly due to the high compatibility of dextran and less toxic elements the NCs contain.

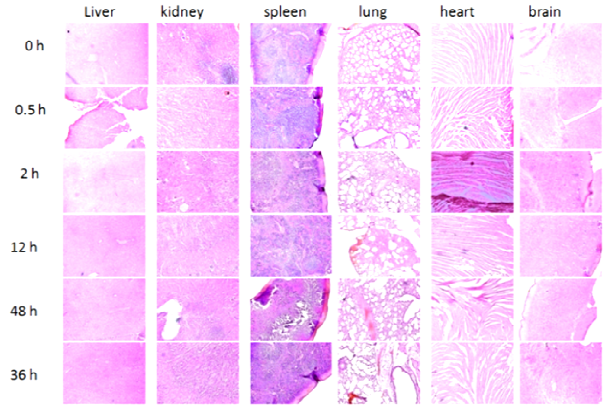

Fig. 4 H&E staining of liver, kidney, spleen, lung, heart and brain tissues harvested at indicated time points after injection with dextran-coated $KMnF_3$ NCs (5mmol/kg dosage). The samples collected at the 0 h points are the control group without injection of NCs.

Considering that dextran-coated nanocubes were applied as an intravenously injected agent, we need to address the possible hemo-toxicity of this exogenous probe. Hemo-toxicity was evaluated by a complete set of hematology assay, as shown in Figure 5. The longitudinal monitoring continued for three days due to its retention time in the plasma. The hematology results showed the blood counts were within the normal range through all the tested time point after administration, for example, the number of white blood cell had slight increase within half to two hours after injection, but recovered to the normal level 12 hours later. Dextran-coated $KMnF_3$ NCs showed similar hemo-compatibility to the PEGylation IO nanoparticle tested on the mice except discrepancy timing.[15]

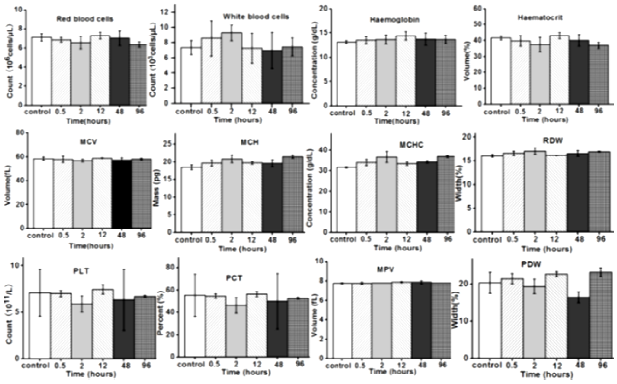

Fig. 5 Hematology of mice administrated with Dextran-coated $KMnF_3$ NCs. Red blood cell number, white blood cell number, hemoglobin concentration, hematocrit, mean corpuscular volume (MCV), mean corpuscular hemoglobin (MCH), mean corpuscular hemoglobin concentration (MCHC), red cell distribution width (RDW) platelets (PLT), platelet hematocrit (PCT), mean platelet volume (MPV) and platelet distribution width (PDW) of miceblood were measured from 0.5 hour to three days after intravenous injection with the Mn dosage of (5 mmol/kg).

Blood chemistry assay is commonly used to determine in vivo toxicity on the organs. We mainly focused on analyzing those enzymes highly related to liver damage. The blood chemistry results, as shown in Figure 6, showed time-dependent variation of biochemical indexes associated with liver function after injection of dextran-coated NCs. Among these factors aspartate transaminase (AST), alanine transaminase (ALT) and glutamyl transpeptidase (GGT) that are enzymes mainly associated with the hepatocytes in the liver, were found to increase slightly within two hours after injection and then return to the normal level. Since the nanocubes are taken up in the Kupffer cells in the liver, the capping-organic residue (e.g. oleylamine) might be degraded, which caused enhancement of the AST and ALT levels. Alkaline phosphatase (ALP) was iniatially decreased but recovered after 12 hours, which is also consistent with elevation of bilirubin's concentration. Other blood indexes for renal function were within the normal range (data not shown). The blood chemistry result behaved similarity as a previous report with pluronic-coated IO nanocomposites tested in rats, including the response timing.[16] Overall, the data of toxicity, bio-distribution, histopathology, hematology, and blood chemistry of the dextran-coated $KMnF_3$ nanocube suggest its favorable biocompatibility. Taking advantage of the fact that the nanocubes are predominant taken up by liver, and applied for in vivo MRI hepatic cancer detection, we established two typical animal models of liver cancer: chemical-induced HCC and CRC liver metastases, to assess the potential utility of dextran-coated $KMnF_3$ NCs for detection of both types of liver cancer. As described in the experimental procedures, primary liver tumor was successfully induced by feeding the mouse with diethylnitrosamine (DEN), which recapitulate the early stage of human liver tumor.[17] Colorectal liver metastases model was established by injecting SW480 human colorectal cancer cells into spleen, which metastasize via the splenic vein to form liver metastases, as occurred in the patients.[18] It is clinically difficult to detect the early stage of liver cancer or metastasis progression by MRI due to their small sizes. Clinically detectable lesions are typically over a centimeter in diameter. After administration of the contrast agents, normal liver tissues were enhanced on T1-weighted images, whereas the contrast of cancer lesions remains unchanged due to its lack of MPS system to phagocytes the contrast agents. Differentiation of the NP's uptake resulted in a clear tumor contrast. Therefore, the contrast-enhanced MRI is useful for diagnosis of both types of liver cancer.

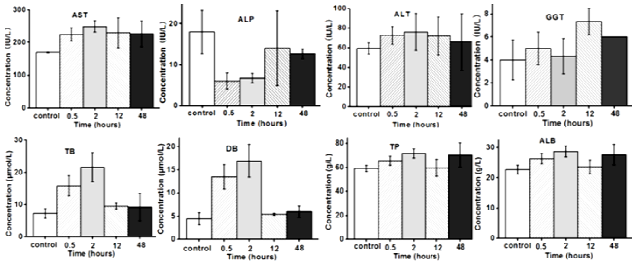

Fig. 6 Liver disease-related blood chemistry of mice injection of on concentration of dextran-coated $KMnF_3$ NCs. Aspartate transaminase (AST), alkaline phosphatase (ALP), alanine transaminase (ALT), glutamyl transpeptidase (GGT), total bilirubin (TB), direct bilirubin(DB), total protein (TP), serum albumin (ALB) mice 0.5 hours to three days after intravenous injection with the dosage of 5 mmol Mn/kg).

To evaluate the efficacy of dextran-coated $KMnF_3$ NCs on enhancing MRI contrast of hepatic lesions, in vivo MR imaging was conducted on a 3 T human scanner with a proper animal coil. To increase the spatial resolution the slice thickness was set as the minimal value of 0.6 mm although the signal noise ratio (SNR) was compensated. T_1-weighted MR images were acquired before and after intravenous administration of 5 mmol Mn/kg of the NCs into the mice bearing liver cancer. As expected, most of the lesions were undetectable, while only a few of them were obscurely visualized on pre-contrast MRI (Figure 7), By contrast, after administration the cancer tissues in the liver appeared as dark spots on the T_1-weighted MR images, whereas surrounding normal tissues with particle accumulations were hyperintense, as clearly seen in Figure 7. Even the lesions as small as 0.4 mm in diameter, their shapes and boundaries were clearly defined by viewing the image. For these metastatic lesions that have normally irregular shapes, their boundaries are still ascertained. Note that although some reports demonstrated that enhancing effect is due to the ions released from the NPs,[19] in this report we considered the NP itself is the effective species as it maintain highly stable in the similar pH surrounding since no free ions can be detected and its morphology keeps unchanged (data not shown here). By comparison we also performed contrast enhancement MRI with the commercial MnDPDP on the metastatic hepatic cancer mouse model. Much less tumor contrast than that of dextran-coated $KMnF_3$ NCs was achieved with MnDPDP, as shown in Figure S3. To validate the MRI findings, pathological examination was performed on the liver sections of the mice. All the sections contained small cancer lesions or metastasis in the liver (Figure S4), correlating well with those seen on MRI. Current imaging methods rarely detect the early progression of primary or spread of metastatic liver cancer, which prohibits early and most likely effective interventions, for example, micrometastases (0.2-2mm in size) can rarely be detected based on changes in perfusion by radionuclide imaging or Doppler perfusion techniques. Clinically five-year survival rate of primary liver tumor after excision can be as high as 80% if the lesion size is smaller than 2 cm. Our results have clearly proved that dextran-$KMnF_3$ NCs are applicable for early diagnosis of primary or metastatic liver cancer, which lays foundation for ultimate clinical translation.

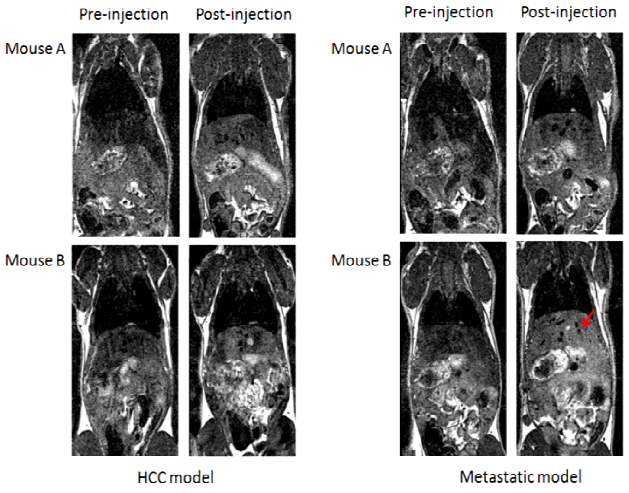

Fig. 7 Typical MR Images of the mice bearing primary or metastatic liver cancer, Thirty minutes after administration of dextran-coated $KMnF_3$ NCs (5mmol Mn/kg dosage for each mouse). Two mice were randomly chosen for each type of liver cancer. All the lesions have the size ranged from 0.4mm to 2 mm (e.g. the lesion pointed by red arrow points is 0.8 mm). Note that metastatic lesions typically have irregular shape, as compared to the relatively spherical primary lesions.

Conclusions

In summary, biocompatible dextran-$KMnF_3$ NCs were synthesized by a simple solution method. Those NCs are not only compatibility with liver cells, but also display high hemo-compartibility and proper plasma life-time. Moreover, they are capable of shortening T_1 relaxation time of excited hydrogen, as applied for MR imaging of hepatic lesion in vivo, they evidently enhanced the contrast of the lesion in the liver, either for primary cancer or metastatic cancer. Our results indicated great potential of dextran-$KMnF_3$ NCs for biomedical imaging. Expanded investigations of the utility of NCs on the diagnosis of other liver cancers by MRI are currently in progress.

Acknowledgment

This work is financially supported by the National Natural Science Foundation of China (21361018), the Fundamental Research Foundation of the Jiangxi Ministry of Education (GJJ14123) and National Key Technology Research and Progression Program of the Ministry of Science and Technology of China (2012BAE01B02). The authors acknowledge Dawen Zhao (UT Southwestern Medical Center), Xiao-zeng You (Nanjing University) and Jian-qi Li (Shanghai Key Lab of Magnetic Resonance) for helpful discussion and in-vivo MRI operation.

Notes and references

[a]*Institute for Advanced Study, Nanchang University, NO. 999 Xuefu Avenue, Honggutan District, Nanchang 330031, China. Fax:+86-791-83969963.Telephone: +86-791-83969964. Email: tangqun@ncu.edu.cn.*

[b]*Key Laboratory of Functional Small Organic Molecules, Ministry of Education and College of Life Science, Jiangxi Normal University, Nanchang 330031, China.*

† Electronic Supplementary Information (ESI) available: [Hydrodynamic diameter distribution curve, typlan blue staining, MnDPDP enhanced MRI, H&E staining liver cancer]. See DOI: 10.1039/b000000x/

1 (a) R. Weissleder and M. J. Pittet, *Nature* 2008, **452**, 580; (b) B. Z. Qian and J. W. Pollard, *Cell* 2010, **141**, 39.

2 (a) F. Hyafil, J. Cornily, E. Feig, J. R. Gordon, E. Vucic, V. Amirbekian, E. A. Fisher, V. Fuster and L. J. Feldman, Z. A. Fayad, *Nature Med.* 2007, **13**, 636; (b) R. Weissleder, M. Nahrendorf and M. J. Pittet, *Nature Mater.* 2014, **13**, 125.

3 (a) Z. Cheng, Y. Cheng, X. Kang, C. Li, S. Huang, H. Lian, Z. Hou, P. Ma and J. Lin. *Biomaterials*. 2014, **35,** 6359; (b) N. Nasongkla, E. Bey, , J. M. Ren, H. Ai, C. Khemtong, J. S. Guthi, S. F.Chin, A. D.Sherry, D. A. Boothman and J. M. Gao, *Nano. Lett*. 2006, **6**, 2427; (c) P. D. Garimella, A. Datta, D. W. Romanini, K. N. Raymond and M. B. Francis, *J. Am. Chem. Soc*. 2011, **133**, 14704.

4 (a) D. D. Stark, R. Weissleder and G. Elizondo, *Radiology* 1988, **168**, 297; (b) C. Tassa, S. Y. Shaw and R. Weissleder, *Acc. Chem. Res.* 2011, **44**, 842.

5 Y. X. Wang, *J. Quant. Imaging. Med. Surg.* 2011, **1**, 35.

6 A. Schroeder, D. A. Heller, M. M. Winslow, J. E. Dahlman, G. W. Pratt, R. Langer, T. Jacks and D. G. Anderson, *Nat Rev Cancer*. 2011, **12**, 39.

7 (a) E. A. Murphy, B. K. Majeti, L. A. Barnes, M. Makale, S.M. Weis, K. Lutu-Fuga, W. Wrasidlo and D. A. Cheresh, Proc. Natl. Acad. Sci. U.S.A. 2008, **105**, 9343; (b) P. M. Peiris, R. Toy, E. Doolittle, J. Pansky, A. Abramowski, M. Tam, P. Vicente, E. Tran, L. Hayden, A. Camann, A. Camann, A. Mayer, B. O. Erokwu, Z. Berman, D. Wilson, H. Baskaran, C. A. Flask, R. A. Keri and E. Karathanasis, *ACS NANO* 2012, **6**, 8783.

8 A. Salvati, A. S. Pitek, M. P. Monopoli, K. Prapainop, B. F. Baldelli, D. R. Hristov, P. Kelly, C. Åberg, E. Mahon and K. A. Dawson, *Nature Nanotech.* 2013, **8**, 137.

9 (a) H. B. Na, J. H. Lee, K. An, Y. I. Park, I. S. Lee, D.H. Nam, S. T. Kim, S.H. Kim, S.W. Kim, K. H. Lim, K. S. Kim, S. O. Kim and T. Hyeon *Angew. Chem., Int. Ed.* 2007, **46**, 5397; (b) J. L. Bridot, A.C. Faure, S. Laurent, C. Rivière, C. Billotey, B. Hiba, M. Janier, V. Josserand, J. L. Coll, L. V. Elst, R. Muller, S. Roux, P. Perriat and O. Tillement *J. Am. Chem. Soc.* 2007, **129**, 5076. (c) X. J. Kang, Z. Y. Cheng, D. M.Yang, P. A.Ma, M. M. Shang, C. Peng , Y. L. Dai and J. Lin, *Adv. Funct. Mater*.2012, **22**,1470.

10 (a) Z. Liu, X. Song and Q. Tang, *Nanoscale* 2013, **5**, 5073; (b) Z. Liu, X. Song, X. Xu and Q. Tang, *Nanotechnology*, 2014, **25**, 155101; (c) X. Song, Z. Liu, X. Xu and Q. Tang, *New, J. Chem.* 2014, **38**, 3813.

11 K. I. Shingel, *Carbohydrate Research* 2002, **337**, 1445.

12 (a) S. M. Hussain, K. L. Hess, J. M. Gearhart, K. T. Geiss and J. Schlager, *J. Toxicology in Vitro* 2005, **19**, 975; (b) P. P. Fu, Q. S. Xia, H. M. Hwang, P. C. Ray and H. T. Yu, *Journal of Food and Drug Analysis* 2014, **22**, 64.

13 (a) D. A. Bass, J. W. Parce, L. R. Dechatelet, P. Szejda, M. C. Seeds and M. Thomas, *J. Immunol.* 1983, **130**, 1910; (b) E. Herzog, H. J. Byrne, M. Davoren, A. Casey, A. Duschl and G. J. Oostingh, *Toxicology and Applied Pharmacology* 2009, **236**, 276.

14 (a) S. T. Reddy, A. J. van der Vlies, E. Simeoni, V. Angeli, G. J. Randolph, C. P. O'Neill, L. K. Lee, M. A. Swartz and J. A. Hubbell, *Nature Biotechnology* 2009, **25**, 1159; (b) C. Hanley, A. Thurber, C. Hanna, A. Punnoose, J. H. Zhang and D. G. Wingett, *Nanoscale Research Letters* 2009, **4**, 1409; (c) Y. F. Li and C. Y. Chen, *Small*, 2011, **7**, 2965.

15 G. Luo, R. H. Fang, M. J. Sailor and J. H. Park, *ACS Nano.* 2012, **6**, 4947.

16 T. K. Jain, M. K. Reddy, M. A. Morales, D. L. Leslie-Pelecky and V. Labhasetwar, *Mol. Pharmaceutics* 2008, **5**, 316.

17 A. Schmid, B. Rignall, B. J. Pichler and M. Schwarz, *Toxicological Sciences* 2012, **126**, 52.

18 W. S. Wang, P. M. Chen, H. L. Hsiao, H. S. Wang, W. Y. Liang and Y. Su, *Oncogene* 2004, **23**, 6666.

19 (a) F. B. Margaret, L. L.Tricia, K. N. Michael, U. Gözde, W. B. Gary and M. S. Erik, *ACS Nano* 2011, **5**, 3438. (b) E. M. Shapiro and A. P. Koretsky, *Magn. Reson. Med.* 2008, **60**, 265.